# Modeling thin layers of analytes on substrates for spectral analysis: use of solid/liquid *n* and *k* values to model reflectance spectra

Bruce E. Bernacki
Timothy J. Johnson
Tanya L. Myers

SPIE.

# Modeling thin layers of analytes on substrates for spectral analysis: use of solid/liquid *n* and *k* values to model reflectance spectra

**Bruce E. Bernacki,\* Timothy J. Johnson, and Tanya L. Myers**
Pacific Northwest National Laboratory, Richland, Washington, United States

**Abstract.** Since solids are only sometimes seen *en masse* in a pure bulk form, and for liquids other than water almost never, a capability to model reflectance spectra from analytes deposited on various substrates would be highly advantageous. If available, the real, $n(\nu)$, and imaginary, $k(\nu)$, components of the complex refractive index, $\tilde{n} = n + ik$, can be used to simulate infrared spectra, accounting for reflection, refraction, and absorption phenomena as a function of wavelength. We focus on using the Pacific Northwest National Laboratory (PNNL) derived $n/k$ vectors for solid and liquid analytes deposited as thin layers on different types of substrates including conductors, such as aluminum, and inorganic dielectrics, such as glass. The model is an adaptation of the Monte Carlo ray trace modeling program, TracePro, extended through the use of its macrolanguage. The model is tested using thin films of organic liquids including silicone oil and no. 2 diesel fuel, as well as organic solids such as caffeine and acetaminophen on aluminum and glass. The predicted spectra for the solid films were compared to experimental hemispherical reflectance data measured using a Fourier transform spectrometer with an integrating sphere. The thickness of the calculated layer is a parameter for predicting the (transflectance) spectra and is obtained using the areal density measured from gravimetric methods to generate the thin-layer samples. Comparison of the calculated spectra with experimental hemispherical reflectance data shows excellent agreement, indicating promise for the use of measured $n/k$ data to synthesize reference spectral data. In particular, accounting for the inhomogeneity of the deposits greatly improved the match with experimental data. Finally, the theoretical modeling shows that for thicker layers (ca. 20 to 100 $\mu$m) of typical organics possessing moderately strong $k$ values, the longwave infrared features are often saturated and better spectral contrast is obtained from the overtone/combination bands in the shortwave infrared. © *The Authors. Published by SPIE under a Creative Commons Attribution 4.0 Unported License. Distribution or reproduction of this work in whole or in part requires full attribution of the original publication, including its DOI.* [DOI: 10.1117/1.OE.59.9.092005]

## 1 Introduction

Spectroscopy, especially infrared absorption and reflectance spectroscopy, is a valuable tool to remotely detect and identify unknown gases,[1–4] solids,[5–7] and liquids.[8,9] Identification of unknown spectra from library endmembers makes use of techniques such as matched filtering, generalized least squares, and mixture-tuned matched filtering.[10] In all of these methods, it is necessary to have a spectrum of the unknown material in the library for reliable identification. Spectral libraries exist for the three phases of matter, with solid materials typically characterized using reflectance spectroscopy, and gases and liquids identified predominantly using absorption spectroscopy.[10,11] Unlike gases, the ability to detect solids and liquids under various environmental conditions using spectroscopic techniques can be challenging since morphological phenomena such as layer thickness,[12] substrate composition,[13,14] or particle size[15,16] are all known to affect the infrared reflectance, emission, and transmission spectra. Generating a spectral library

---

\*Address all correspondence to Bruce E. Bernacki, E-mail: bruce.bernacki@pnnl.gov

with all the different morphological conditions would require an infinite number of measurements; modeling the solid or liquid spectrum to account for the different morphological conditions is thus preferred but requires both the real ($n$) and imaginary ($k$) optical constants of the complex refractive index where $\tilde{n} = n(v) + ik(v)$.

Identification of endmembers obtained via imaging spectroscopy is traditionally accomplished by comparing the unknown library endmember spectra found via reflectance spectroscopy using various algorithms.[10,17] However, experience has shown there can be differences between field-obtained data and laboratory-measured spectra of neat chemicals. Consequently, there has been recent interest in obtaining the complex index of refraction of materials from which reflectance versus wavelength (or wavenumber) data can be calculated by way of the Fresnel equations for bulk materials or using ray tracing or thin film calculations. However, for many materials of environmental or security interest, such as explosives, chemical agents, or their precursors, the chemicals exist most often only as thin films either on metal or dielectric substrates. The combination of thin films of either solids or liquids on surfaces can result in complex spectra that contain attributes of both the film material and substrate.

In the complex index of refraction, the real part $n(\nu)$ describes the material's reflectance and refraction properties, and the imaginary part $k(\nu)$ describes the attenuation of light within the medium.[18] In the infrared, these properties are associated with the spectroscopic rotational–vibrational features that are useful in identifying materials such as organic gases or liquids, especially within the molecular fingerprint region spanning 5.5 to 25 $\mu$m. Once the complex index of refraction is found, the bulk reflectance from the first surface of the material can be calculated using the Fresnel equations.[18] Since liquids as well as most solid deposits will only rarely be seen in pure bulk form, one is more likely to see the influence of the substrate combined with that of the liquid or solid, and this composite signature may not necessarily strongly resemble either signature. However, using the complex index of refraction for both the material and substrate, reflectance spectra can be calculated and eventually matched to acquired endmember data with a good degree of confidence. In the following, the methods used to model various liquid and solid thin films are described, along with assumptions about the liquid, solid, and substrate. Finally, modeling results of selected liquids and solids on metal and dielectric substrates are presented, including rough (scattering) metallic substrates.

## 2 Experimental Methods

The theoretical calculations presented here are all based on using $n(\nu)$ and $k(\nu)$ vectors to perform the calculations, and in most cases the calculated spectra are compared to experimental directional-hemispherical reflectance spectra recorded using an integrating sphere coupled to a Fourier transform infrared spectrometer. The $n(\nu)$ and $k(\nu)$ vectors that are used in the models described here were obtained from the PNNL database of optical constants.[8,19,20] This database consists of a set of $n/k$ spectra for a rather large collection of liquids of different chemical varieties: organics, inorganics, polar, nonpolar viscous, etc. The liquids $n/k$ data[8] were derived using improved methods originally developed by Bertie et al.,[21,22] whereby a series of absorption spectra are recorded from liquid cells of fixed path lengths, and the scalar refractive index $n$ is also measured using an Abbe refractometer. The Kramers–Kronig transform uses these data to iteratively generate the $n/k$ vectors. The PNNL data set also consists of a set of $n/k$ data for solids, data which are, in general, much more difficult to obtain; most of the experimental details of the methods to obtain the $n/k$ data for the solid samples have been previously reported as obtained by any of three methods: single-angle reflectance spectroscopy,[23,24] ellipsometry,[25,26] or a more economical method,[27] whereby the $k$ values are obtained from the absorbance data of KBr pellets prepared using quantitative gravimetric analysis. In the KBr pellet method, the $n$ values are calculated from $k(\nu)$ by Kramers–Kronig transformation along with an approximated scalar value of $n$ at the high wavenumber limit of $k(\nu)$. Both liquid and solid thin films are examined in this paper.

To obtain the experimentally-derived results, it was necessary to record the directional–hemispherical reflectance spectra.[28] The measured total hemispherical reflectance (diffuse + specular) is reported in many of the following examples. These data were recorded using a 75-mm sphere

with a nominally matte gold interior surface (Bruker A 562) and a Fourier-transform infrared (FTIR) spectrometer. The FTIR (typically either a Bruker Tensor 37 or Matrix IR cube) was used with the infrared beam coupled to the inlet port of the sphere.[28] Both FTIRs were operated in the mid-IR using a SiC source, KBr beamsplitter, and an HgCdTe detector with a spectral resolution of 4 cm$^{-1}$.

The thin layer solid samples for the reference measurements were provided and prepared by the Johns Hopkins University Applied Physics Laboratory (APL). Soda lime glass substrates were used without any surface modification, but roughened aluminum substrates were prepared via grit blasting with 150-mesh SiC. Solid analytes were deposited onto the substrates via robotic airbrushing of the chemicals from solution.[29] Final mass loading was controlled through solution concentration and volume of the solution deposited onto the samples and verified by gravimetric analysis. A Keyence VHX-1000 digital microscope was also used to record high-quality photomicrographs of the various samples to examine the uniformity of the layers. Images for the solid samples on glass and polished aluminum are presented but not for samples on roughened aluminum since the surface roughness was too high ($\sim$2 $\mu$m) compared to the film thickness, making it impossible to yield information regarding the uniformity. For the liquids, spin coating was used to apply thin films to the substrates but attempts to quantify the thickness of the analytes were not successful;[30] reference measurements are thus not presented for the liquids.

## 3 Modeling Approach

In this paper, a Monte Carlo ray tracing program (TracePro)[31] is used to model liquid films on substrates with nonsequential ray tracing using a substrate + thin layer model. The ray-tracing approach treats light incoherently (i.e., phase is not considered), which is not unreasonable for real-world data acquisition. TracePro, which can assign both material as well as surface properties of the substrate, can extend modeling into a regime where scattered light is detected from a surface using either bidirectional reflectance distribution function (BRDF) models or measured scattering data. However, scattering was not considered in any of the modeling results presented in this paper. An additional consideration is that a ray-tracing approach such as that used in this study has the ability to create more complex spatial models in which thin films with voids or droplet models can be considered, as well as homogeneous but nonuniform thickness of thin layers.

It is worth noting that traditional thin film modeling methods, such as the transfer matrix method (TMM),[32] have the ability to model basic systems by providing an exact solution to Maxwell's equations. However, TMM models require assumptions such as an infinite substrate, and homogeneous, parallel film layers; TMM cannot address scattering from very rough surfaces or model films with voids or droplets nor analyze nonuniformly thick layers, which TracePro® can. We plan to pursue such studies in the future.

The liquids examined include no. 2 diesel fuel and silicone oil. Substrates considered include aluminum and soda lime glass. These provide a small subset of organic liquids and substrates to illustrate the challenges of detecting thin absorbing layers of liquids on either metallic or dielectric surfaces. In addition, thin layers of solid materials are also considered for which $n$ and $k$ values have been derived using the KBr pellet method.[27] In the case of the solids, these materials are applied to aluminum and glass substrates with known areal density (and hence, known film thickness) in order to validate the modeling approach, or in some cases, show where there are challenges in practice and more research is needed.

## 4 Reflectance of Liquid Films on Substrates

### 4.1 *Substrates*

Both aluminum[33] and soda lime glass[34] substrates are considered for these modeling efforts. Figure 1 plots the complex index of refraction for both substrates. In comparison to aluminum, significant variation in $n$ and $k$ for soda lime glass is evident throughout the wavelength region
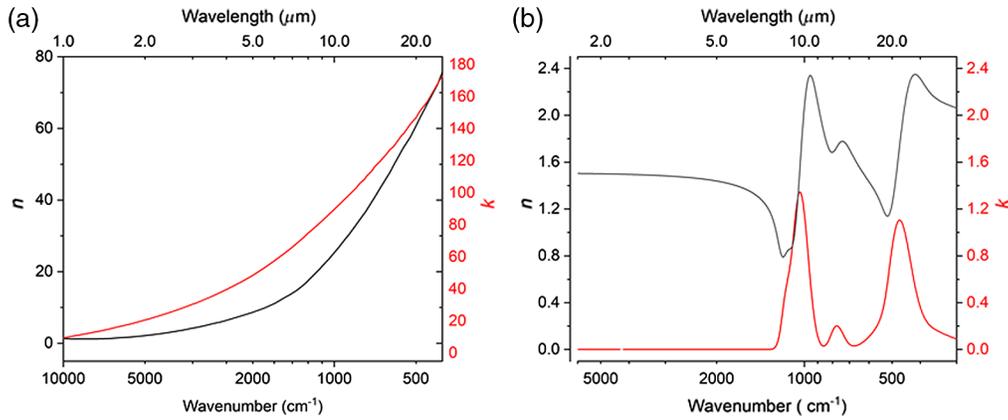
**Fig. 1** Complex index of refraction plots for (a) aluminum and (b) soda lime glass. The real component $n$ is plotted in black on the left axis, the imaginary component $k$ in red on the right axis.
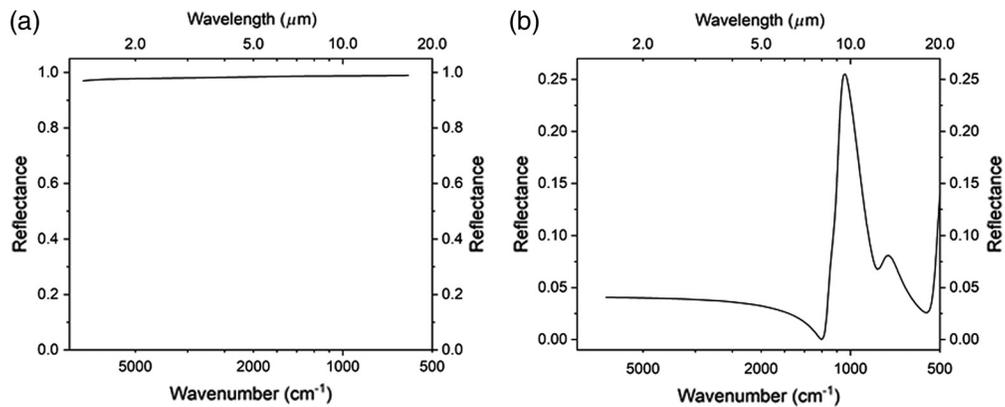


**Fig. 2** Modeled reflectance versus wavenumber (wavelength) is shown above for (a) bare aluminum and (b) bare soda lime glass.

of interest. All reflectance plots shown in this paper are calculated with unpolarized illumination at $+15$ deg and light collected at the specular angle of $-15$ deg.

Once a researcher has access to the complex index of refraction, reflectance data can be calculated; Fig. 2 displays the first surface or bulk reflection plots for both aluminum and soda lime glass. Aluminum displays the high reflectance common to most metals and is relatively featureless spectroscopically, while soda lime glass exhibits relatively low reflectance except for the peak around 10 $\mu$m due to the Si–O antisymmetric stretch.

### 4.2 Liquid Layers on Metal Substrate

Next, the addition of liquid layers is examined on the aluminum and soda lime glass substrates. The two liquids considered are silicone oil and no. 2 diesel fuel, whose complex index of refraction plots[20] are shown in Fig. 3. The strongest feature for silicone oil occurs at 802 cm$^{-1}$ with a peak $k$-value of 0.9 and is due to the Si–C stretch. Weaker $k$-values are observed for no. 2 diesel fuel in which the strongest features occur in the C–H stretching region with a smaller peak $k$-value of $\sim$0.13 at 2925 cm$^{-1}$.

Using the $n$ and $k$ values shown in Fig. 3, first surface or bulk reflectance values are computed for infinitely thick layers of silicone oil and no. 2 diesel fuel. The reflectance values are shown in Fig. 4. The bulk spectra resemble the real part of the refractive index since the illumination is completely attenuated by the liquid and the substrate has no influence on the spectral response.
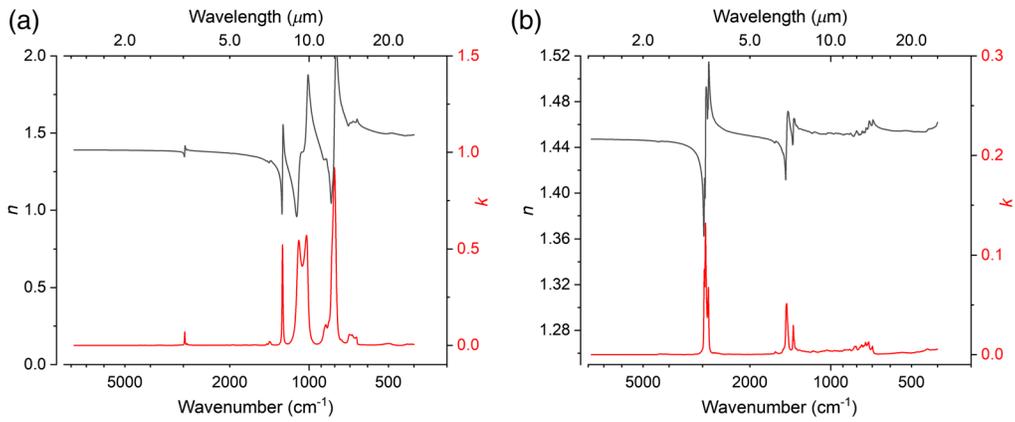
(a)



(b)



**Fig. 3** Experimental complex index of refraction plots for (a) silicone oil and (b) no. 2 diesel fuel versus wavenumber (wavelength). The real component $n$ is plotted in black on the left axis, the imaginary component $k$ in red on the right axis.
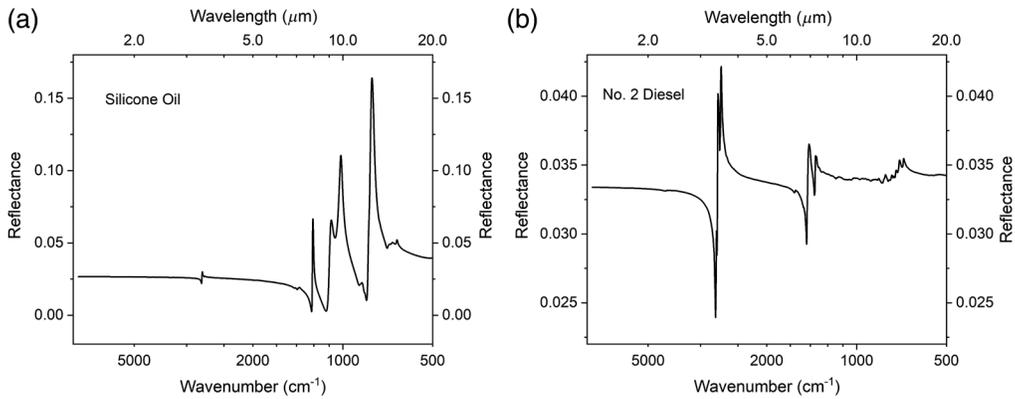
(a)



(b)



**Fig. 4** Modeled first surface reflectance of bulk liquid samples of (a) silicone oil and (b) no. 2 diesel fuel versus wavenumber (wavelength).

When thin films of silicone oil having layer thicknesses of 1 and 100 $\mu$m, respectively, are layered atop an aluminum substrate, the transflectance plots shown in Fig. 5 are determined. It is worthy to note the marked difference in the two spectra: for the thin layer, the spectrum resembles a double-pass absorption spectrum with near Beer–Lambert behavior, whereas for the thicker 100-$\mu$m layer, as the film layer increases, those portions of the modeled response in the
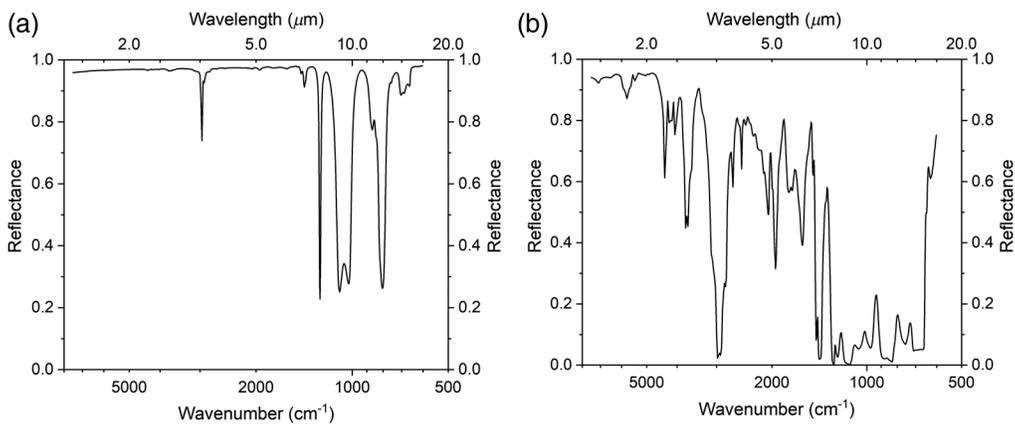
(a)



(b)



**Fig. 5** Modeled reflectance versus wavenumber (wavelength) for (a) 1 $\mu$m of silicone oil on aluminum and (b) 100 $\mu$m of silicone oil on aluminum.
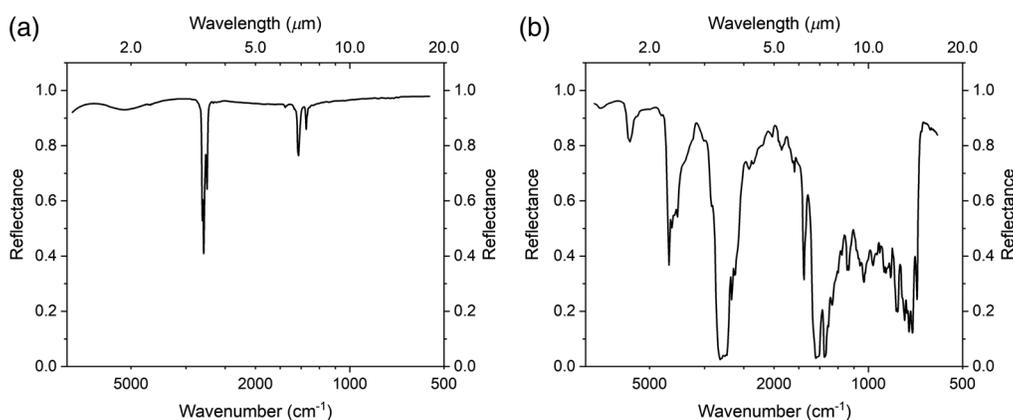
**Fig. 6** Modeled reflectance of no. 2 diesel fuel on aluminum for layer thicknesses of (a) 1 $\mu$m and (b) 100 $\mu$m. As was seen in Fig. 5, as the film layer thickness increases, portions of the trans-flectance spectrum become saturated in regions of high $k$ values resulting in only first-surface reflection from the film layer reaching the detector.

longwave infrared (LWIR) saturate, and only first surface reflections from the film layer are detected; these regions slightly resemble bulk reflectance of silicone oil [cf. Fig. 4(a)].

For the case of the 1-$\mu$m layer, distinguishable absorption features appear in the reflectance data, but due to the transflectance behavior of the highly reflecting substrate, the response resembles neither the first surface nor the bulk reflectance of silicone oil. As the layer increases to 100 $\mu$m, portions of the transflectance plot saturate. Namely, in the LWIR where the $k$ values are large due to allowed fundamental vibrational transitions, some of the incident light does not reach the aluminum substrate, revealing portions of the spectrum that consequently display only the first surface reflectance of silicone oil. By knowing the complex index of refraction of both the substrate and liquid layers, one can recreate the liquid layer–substrate system and estimate the thickness of the liquid layer. To make identification easier, the data in Fig. 5 suggest that instead of searching in the LWIR where the strongest signatures reside, it may be more advantageous to look for data signatures in the shortwave infrared (SWIR), for example, where greater spectral contrast is observed.

Figure 6 shows modeled reflectance spectra for no. 2 diesel fuel for both 1 and 100 $\mu$m layer thicknesses, with results similar to those shown for silicone oil, but with less pronounced effects as its $k$ values are nearly an order of magnitude smaller than those of silicone oil. The spectra of the two layers as well as the bulk spectrum are still quite different, presenting a challenge for material identification if only the spectrum for the bulk liquid were included in the spectral library. By having the complex index of refraction along with modeling methods, one can investigate optimal regions for detection as well as avoid regions where complete saturation is observed that would confound identification.

### 4.3 Liquid Layer on Dielectric Substrate

In this section, the behavior of thin liquid layers on dielectric substrates is examined. Unlike the aluminum substrate, which has high reflectance and no substantial spectral features, the dielectric medium considered here, soda lime glass, has significant spectral features in the same spectral domain as those of the liquids under study. This results in both different and more complex behavior than that of the liquid–metal systems for which modeling the substrate + layer system using $n$ and $k$ values is well suited. Figure 7 shows the reflectances modeled for 1 and 100 $\mu$m layers of silicone oil on a soda lime glass substrate.

For both the 1- and 100-$\mu$m layer plots shown in Fig. 7, the reflectance features of silicone oil dominate, but for the thin 1-$\mu$m layer example, these features are interloped by features of the soda lime glass. At 100-$\mu$m layer thickness, however, essentially only the bulk reflectance of silicone oil is observed [cf. Fig. 4(a)].
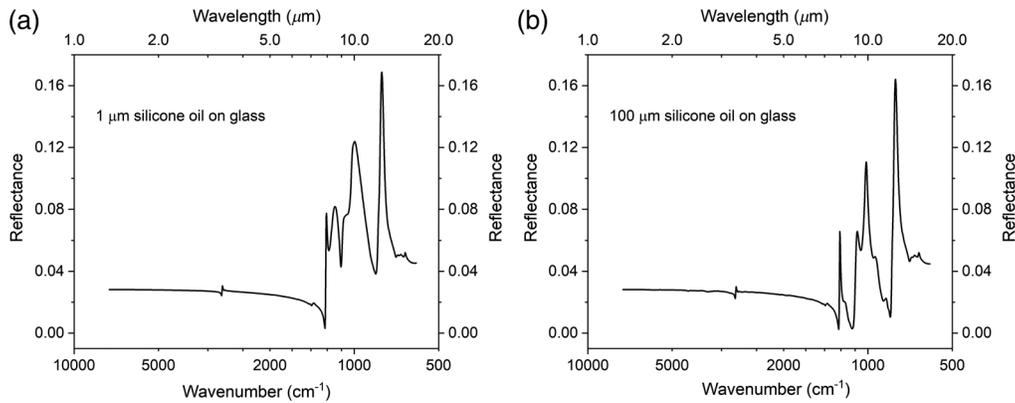
**Fig. 7** Modeled reflectance plots of (a) 1 $\mu$m of silicone oil on soda lime glass and (b) 100 $\mu$m of silicone oil on soda lime glass. Due to the strong absorption features of silicone oil in this wavelength range, the reflectance plot for the 100-$\mu$m case is nearly only the bulk reflectance of silicone oil and minimal signature from the soda lime glass substrate is evident.
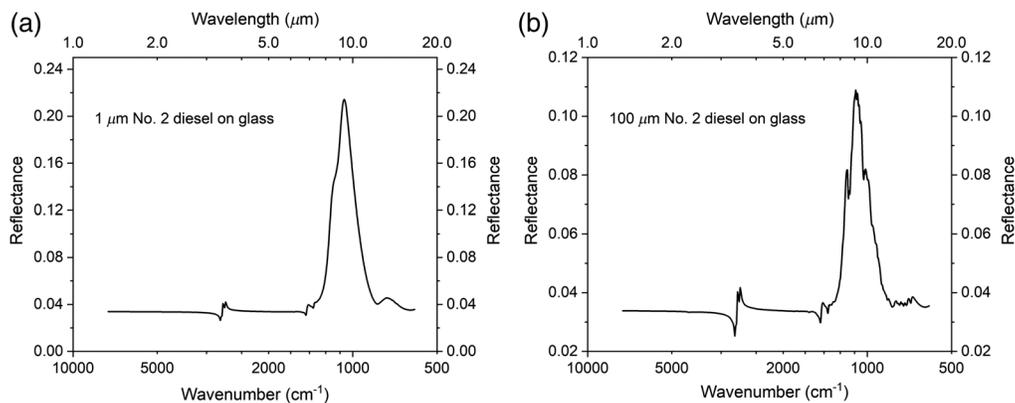


**Fig. 8** Modeled reflectance plots of (a) 1 $\mu$m of no. 2 diesel along with (b) 100 $\mu$m of no. 2 diesel on top of a soda lime glass substrate. In the case of the 1-$\mu$m layer, the glass substrate features dominate.

In a similar fashion, the reflectance of no. 2 diesel fuel, which has smaller $k$ values compared to silicone oil, is explored for 1- and 100-$\mu$m layer thicknesses on soda lime glass, and the results are shown in Fig. 8. In contrast to what was seen for silicone oil, for diesel oil with its smaller $k$ values, the soda lime glass reflectance features essentially dominate with minimal signature of diesel oil in the 1-$\mu$m case. As the layer thickness is increased to 100 $\mu$m, the structured diesel fuel features begin to become evident on top of the soda lime glass reflectance. The features of the soda lime glass, however, are still evident for this thicker layer due to the weaker $k$ values of diesel fuel in contrast to silicone oil [vis-à-vis Fig. 7(b)].

## 5 Reflectance of Solid Films on Substrates

For the case of solid films, samples were provided by APL in which the analytes were deposited on both polished and roughened aluminum substrates as well as soda lime glass.[29] For the materials considered here, the areal density was known at the time of deposition, and with this knowledge together with known volume densities, the thickness of the film layer was calculated and used as input for the model. The substrate characteristics were shown in Sec. 4.1 and will not be revisited. However, micrographs of the samples were recorded with an optical microscope to examine the uniformity of the layers.

The two solids that were modeled include caffeine and acetaminophen. Figure 9 shows the real ($n$) and imaginary components ($k$) of the complex index of refraction for these two analytes
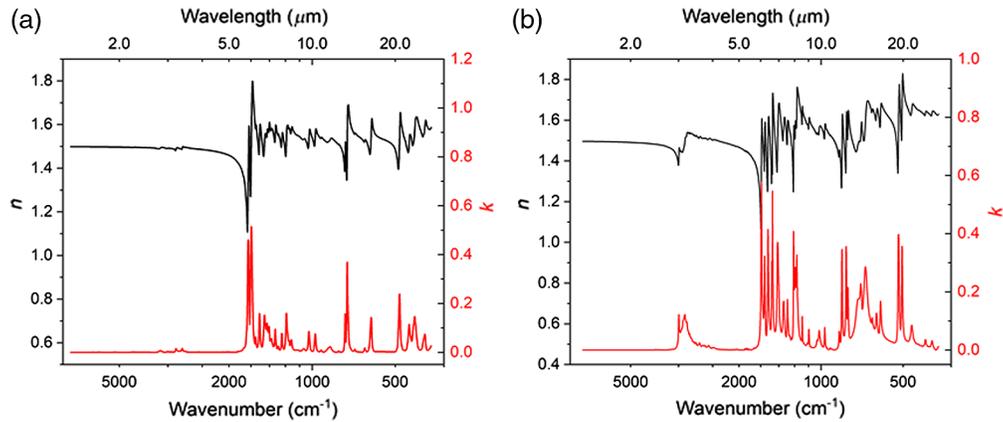
**Fig. 9** Experimental complex index of refraction values ($n$ and $k$) are plotted for (a) caffeine and (b) acetaminophen versus wavenumber.

over the wavelength range of interest. These $n/k$ data were derived from the KBr pellet method.[27]

## 5.1 Caffeine on Aluminum

For the first example, a thin film of caffeine having an areal density of 88.4 $\mu$g/cm$^2$ was applied to polished aluminum. The model requires the physical thickness of the film, which is determined using the volume density[35] of the material and solving for the thickness.

$$\text{thickness} = \frac{\text{areal density}}{\text{volume density}} = \frac{88.4 \times 10^{-6} \text{ g/cm}^2}{1.230 \text{ g/cm}^3} = 7.187 \times 10^{-5} \text{ cm} = 719 \text{ nm}. \quad (1)$$

In Fig. 10, the thin film model reflectance results are compared to experimental measurements of the caffeine film having an areal density of 88.4 $\mu$g/cm$^2$. Good agreement is observed between measured and modeled thin film reflectance when the film thickness is set to 719 nm. Similar results (not shown) were also achieved for a caffeine film prepared with an areal density of 207.2 $\mu$g/cm$^2$ and modeled with a film thickness of 1.685 $\mu$m. The good agreement is indicative of homogeneous deposition of caffeine across the entire substrate without any significant clumping or blank regions as verified by the micrograph image [see Fig. 10(b)], which indicates
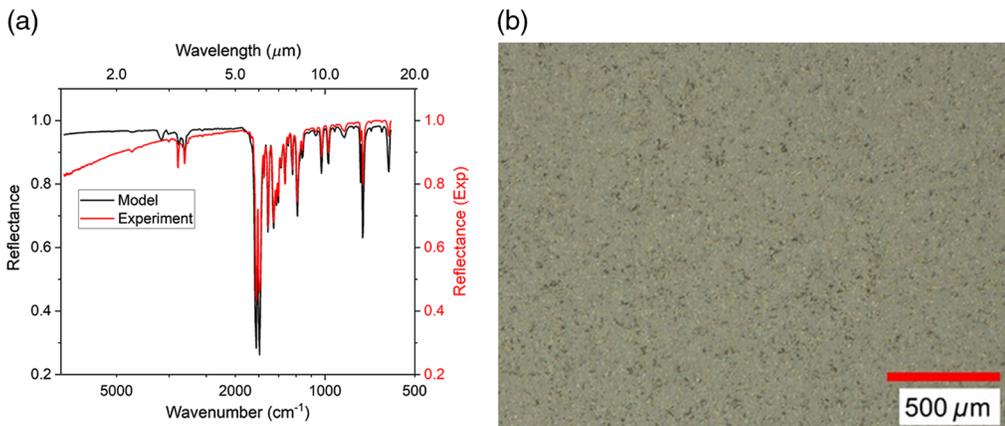


**Fig. 10** (a) Reflectance for a caffeine film having an areal density of 88.4 $\mu$g/cm$^2$ on polished aluminum comparing modeled reflectance (black trace) versus experimental measurements (red trace) along with (b) an image of the deposit recorded with an optical microscope. This areal density corresponds to film thickness of 719 nm.
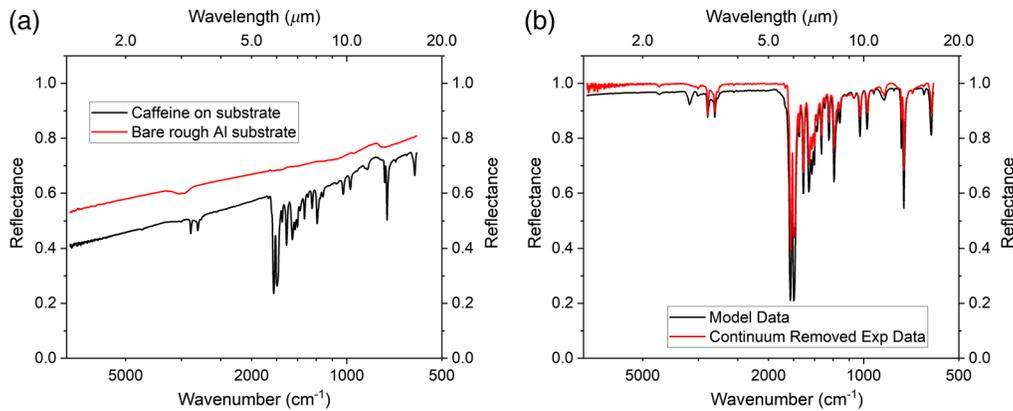
**Fig. 11** (a) Measured reflectance for caffeine with an areal density loading of 106.4 $\mu$g/cm$^2$ on the rough aluminum substrate (black trace) along with measurement of the bare roughened aluminum surface (red trace). (b) To compare the modeled reflectance to the measured value, the measured reflectance was continuum removed and plotted (red trace) against the modeled reflectance (black trace) for the same film thickness.

fairly uniform coverage. As was true for the liquid layer cases, transflectance behavior is seen, but in this case, the layers for the solids were neither thick enough nor so absorptive to cause saturation. For the liquids, saturation was not observed for the thinner 1 $\mu$m layers, which is similar to the thicknesses for the solid films presented in this section.

Additional samples were created and applied in various areal densities to a roughened aluminum substrate created by sandblasting with 150 mesh of SiC grit. The measured reflectance is shown in Fig. 11 for the case of an areal density of 106.4 $\mu$g/cm$^2$ caffeine (a film thickness of 865 nm) on the roughened aluminum substrate compared with the modeled reflectance using the polished aluminum substrate model. The evident wavelength dependence of the reflectance of roughened aluminum (as a substrate) is seen in Fig. 11; it may be due to the surface roughness having an rms roughness of $\sim$2 $\mu$m.[30] Two features are of note: (i) there is a wavelength dependence to the reflectance of the roughened aluminum substrate and (ii) there is an offset between the reflectance of the bare substrate and that of the roughened substrate coated with caffeine. The additional reflective losses arise from the first and second surface reflective losses from the caffeine layer. In addition, the transflectance modulation depth is lower for the areal density than one would obtain using a polished substrate. This may be caused by the reduced reflectance of the aluminum substrate due its roughness, and hence, reduced transflectance.

To compare the modeled and measured data, the measured data had its continuum removed,[36] and the continuum-removed data are compared to the normalized modeled data in Fig. 11. Ideally, one would consider the spectroscopic BRDF of the substrate, but this information was not available, thus the continuum removal method was applied to permit comparison of the modeled and experimental data on a common baseline. In general, the modeled data show greater reflectance magnitude when compared to the measured spectra for this example. Agreement is good across much of the spectrum, although the modeled values slightly overestimate reflectance in general.

## 5.2 Acetaminophen on Aluminum

A second solid material examined was acetaminophen with a density[35] of 1.293 g/cm$^3$. It was also applied to both aluminum and glass substrates with various areal density loadings that were then measured in reflection mode, similar to the methods for caffeine.

The first example of acetaminophen on polished aluminum with an areal density 82.2 $\mu$g/cm$^2$ is shown below (636-nm film thickness). The discrepancy between the experimental and modeled values is stark, which is not surprising upon examining the micrograph of the coated surface in Fig. 12(b). The large discrepancy between the model and experimental data can be explained by the poor homogeneity of the film that exhibits large patches of uncoated aluminum, which skew the measured reflectance data.
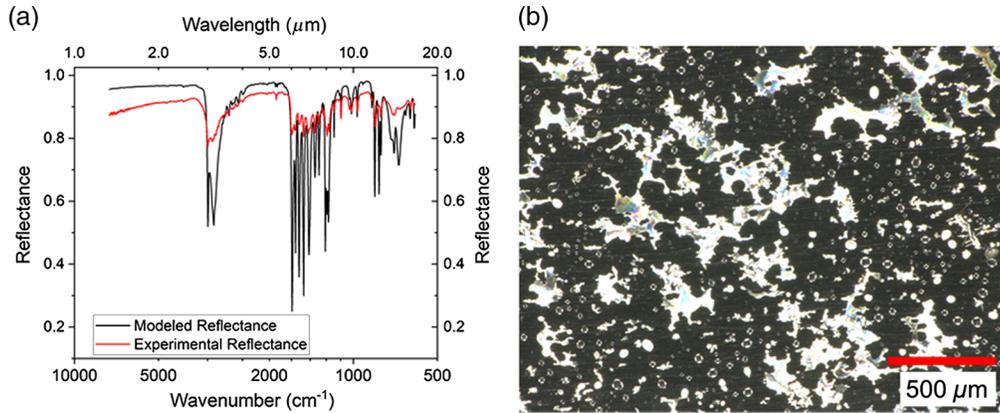
(a)



(b)



**Fig. 12** (a) Modeled and experimental reflectance versus wavenumber (wavelength) for an areal density of 82.2 $\mu$g/cm$^2$ of acetaminophen on polished aluminum along with (b) an image of the deposit recorded with an optical microscope. The acetaminophen analyte corresponds to the white area in the image.

To demonstrate that this "patchy" nature of the coating is the cause of the discrepancy, the above image was made binary and the black pixels counted in order to estimate coverage of the acetaminophen on the aluminum substrate. When compared to the original $1600 \times 1200$-pixel image, only 30% of the pixels were coated. Therefore, a cylindrical thin film layer was created in the model having an appropriate thickness of 636 nm, but having a radius that covered an area of only 30% of the illumination beam's footprint. The results in Fig. 13 show the binarized image along with the new model results compared with the experimental data, exhibiting good agreement between the two cases except for the offset. This offset or reduced reflection from the measured sample arises from scattering from the sample.

As a final example of coating on a metal, a solid thin film of acetaminophen with an areal density of 189.4 $\mu$g/cm$^2$ was coated onto polished aluminum; it is modeled and compared to experimentally measured data in Fig. 14.

As is evident in the image of the film and the experimental reflectance plot, the occurrence of voids decreases the transflectance behavior of the film when compared to an ideal case of a uniform film of 1.46 $\mu$m (corresponding to an areal density of 189 $\mu$g/cm$^2$). Similar to the case shown in Fig. 13, the image of the film was analyzed and coverage or packing density was
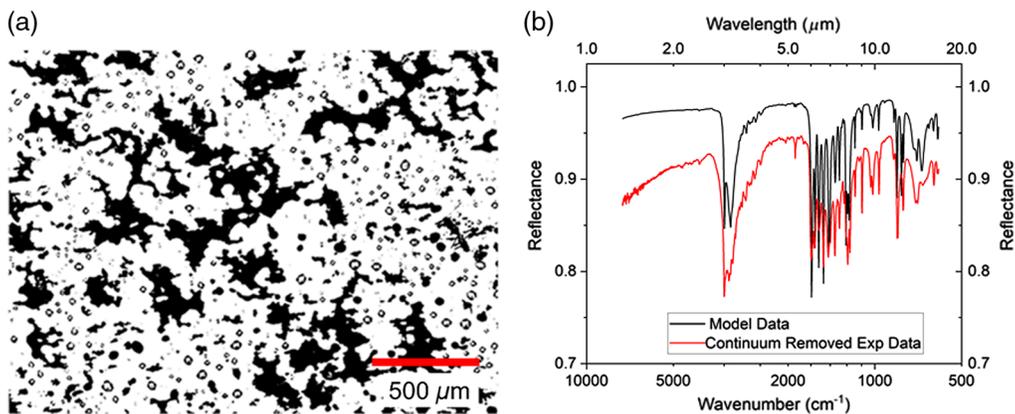
(a)



(b)



**Fig. 13** (a) A binarized version of the image of the acetaminophen film micrograph from Fig. 12 is used to determine the packing density of the analyte compared to the area illuminated by the measurement beam. This information is used in the model to reduce the area of the acetaminophen thin film having the thickness specified by its areal density. This reduced area film is then overfilled by the illumination beam in order to mimic the increased contribution in the experimental data of the bare aluminum substrate in the measured reflectance. (b) This modeled reflectance (black trace) data with a reduced area film is compared to the measured reflectance (red trace) for a film of acetaminophen on polished aluminum.
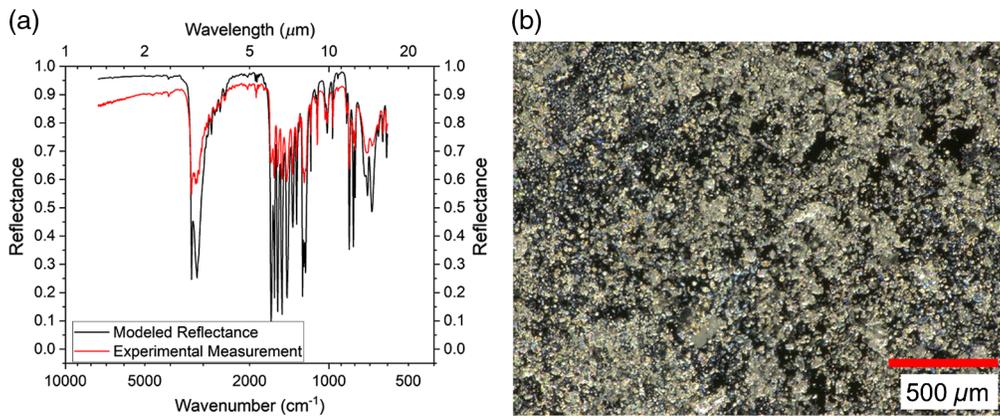
(a)



(b)



**Fig. 14** (a) Reflectance versus wavenumber is shown for modeled (black trace) and experimental (red trace) data along with (b) an image of the coated aluminum substrate. In this example, acetaminophen is coated onto a polished aluminum substrate with an areal density of 189 $\mu$g/cm$^2$, equaling a coating thickness of 1.46 $\mu$m.
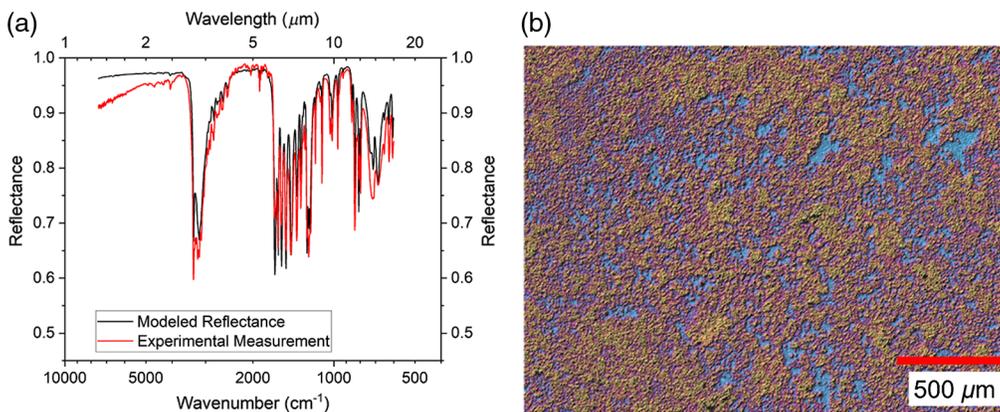
(a)



(b)



**Fig. 15** (a) Modeled (black trace) and measured (red trace) plots of reflectance versus wavenumber for a film of acetaminophen having an areal density of 189.4 $\mu$g/cm$^2$ along (b) with an enhanced image of the film surface. The experimental data are offset slightly to better compare the similarity between the modeled and experimental data. The original image is recolor mapped and plotted using an approach to help visualize the nonuniformity of the coating and void locations. The fill factor is estimated at 45%, and the area of the uniform thin film surface is adjusted accordingly compared to the illumination beam area to approximate the effect of the film voids in a simple manner.

estimated at ∼45%, and a uniform film having an area 45% of the illumination beam footprint was modeled and compared again to the measured reflectance. The final result shown in Fig. 15 shows good agreement between the experimental measurement of reflectance and model when the reduced fill-factor thin film approach is used.

## 5.3 *Acetaminophen on Glass*

As seen in the earlier results for liquids, spectra rapidly become more complex when the substrate also has substantial spectral features within the wavelength range of the measurement. In addition to depositing on aluminum, acetaminophen was also deposited on glass substrates, whose spectra have several spectral features. One such example is shown in Fig. 16 of acetaminophen with an areal density of 226.2 $\mu$g/cm$^2$ (1.750 $\mu$m thickness) on soda lime glass modeled and compared with experimental results. The agreement between the modeled thin film reflectance with experimental measurement is reasonable, except for a slight baseline offset. (Prior measurements determined that a portion of the baseline offset, ca. 3%R, in the measured
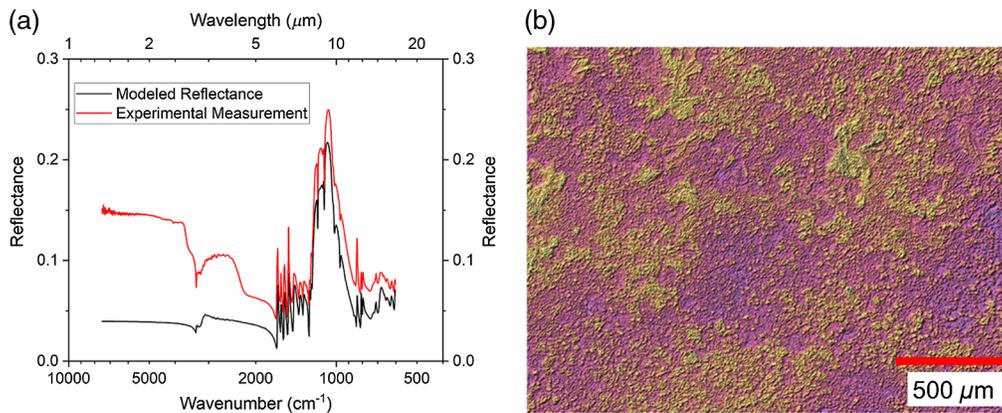
**Fig. 16** (a) Modeled (black trace) and measured (red trace) reflectance versus wavenumber is shown for acetaminophen on a soda lime glass substrate with areal density 226.2 $\mu$g/cm$^2$, which corresponds to a film thickness of 1.750 $\mu$m. (b) An image of the film shows somewhat nonuniform coating, but its effect is less pronounced than the aluminum substrate case.

spectrum is due to the transparency of the substrate such that light is reflected off the Delrin sample holder and detected.) As was true for earlier results of liquid thin films on glass, the spectral features of the soda lime glass dominate and are modulated by those of the analyte acetaminophen. The rough texture of the film on the glass substrate does not seem to have the same negative effect as the aluminum substrate shown in Fig. 12, perhaps because there is less contrast in the reflectance of the analyte compared to the substrate material. Also, with reference to the image in Fig. 16, although the film is patchy, no voids reaching the substrate are apparent.

## 6 Summary and Conclusions

Thin films of liquids or solids on various substrates present challenges to spectral identification owing to the contribution of the substrate's spectral signature combining in a nonlinear fashion with those of the thin films. Historical approaches to spectral endmember identification for either contact or standoff infrared detection[10,17] relied on the application of various algorithms that first removed the spectral effects due to interfering species and then compared the unknown species with library spectra, typically of bulk solids or gases. In the case of thin films, bulk endmember spectra are seldom encountered, and the complex spectra of the thin film/substrate systems require new methods for identification. The availability of the complex index of refraction data in combination with methods such as those described here offers (at the least) a more facile method to compute the reflectance spectra for the bulk material via Fresnel equations, as well as the option to iteratively compute potential spectra of film + substrate systems for multiple candidate materials, including substrates.

Here, we have made initial attempts at modeling these more complex systems with an ultimate goal of synthetically populating all the members of a spectral library using spectra calculated from the Fresnel equations and the associated $n/k$ values versus linear combinations of the two endmembers, namely the pure substrate and the bulk (surface) analyte. Two major classes of thin films were explored: liquids and solids, on both aluminum and glass substrates. Two distinctly different responses were seen in the case of the transflectance that arises from metallic substrates, and the more complex response of thin film materials on soda lime glass substrates. For the case of the solid thin films for which film areal densities were known and experimental reflectance data were available, model results showed good agreement with measured spectra for uniformly covered substrates. Those films for which homogeneous coverage was not achieved showed a marked deviation from model results that assumed even coverage. However, by analyzing images of the films and estimating the fill factor, a lumped model in which the percent coverage was used to postulate a uniform film that incompletely covered the area probed by the model's illumination beam, good agreement could be demonstrated between model and experimental results.

In the case of rough metallic substrates, reasonable agreement between modeled and experimental results was shown when the experimental data had its continuum removed so that it could be compared with the ideal modeled results on a common baseline. Clearly, more work is needed for the treatment of scattering surfaces, but even with good BRDF models, the roughness of the substrates used here was such that it entered the bulk scattering regime, which would be challenging to model without foreknowledge of the substrate.

The modeled results for liquids also highlighted that for thicker layers ($\sim$20 to 100 $\mu$m), the LWIR features are often saturated and display the bulk reflectance in those regions for analytes with moderate to strong $k$ values. Better spectral contrast is obtained from the overtone and/or combination bands in the SWIR. The methods reported here along with the complex index of refraction data thus enable the possibility to optimize detection systems such as spectral range based on the expected analyte, layer thickness, substrate, etc. In conclusion, the use of the complex index of refraction for materials including substrates promises new possibilities for spectroscopic feature extraction, especially for the case of thin films that might be encountered in environmental or defense applications such as the detection of chemical agents or their precursors, or possibly civilian oversight of industrial processes and the detection of toxic industrial chemicals.

## Acknowledgments

## References

1. T. J. Johnson et al., "Absolute integrated intensities of vapor-phase hydrogen peroxide ($H_2O_2$) in the mid-infrared at atmospheric pressure," *Anal. Bioanal. Chem.* **395**, 377–386 (2009).

2. T. J. Johnson et al., "Quantitative IR spectrum and vibrational assignments for glycolaldehyde vapor: glycolaldehyde measurements in biomass burning plumes," *J. Phys. Chem. A* **117**(20), 4096–4107 (2013).

3. M. C. Phillips et al., "Real-time trace gas sensing of fluorocarbons using a swept-wavelength external cavity quantum cascade laser," *Analyst* **139**(9), 2047–2056 (2014).

4. T. Burr and N. Hengartner, "Overview of physical models and statistical approaches for weak gaseous plume detection using passive infrared hyperspectral imagery," *Sensors* **6**(12), 1721–1750 (2006).

5. T. A. Blake et al., "Passive standoff detection of RDX residues on metal surfaces via infrared hyperspectral imaging," *Anal. Bioanal. Chem.* **395**, 337–348 (2009).

6. T. N. Beiswenger et al., "Identification of uranium minerals in natural U-bearing rocks via infrared reflectance spectroscopy," *Appl. Spectrosc.* **72**, 209–224 (2017).

7. T. L. Myers et al., "Hyperspectral imaging of minerals in the longwave infrared: the use of laboratory directional-hemispherical reference measurements for field exploration data," *J. Appl. Remote Sens.* **13**, 034527 (2019).

8. T. L. Myers et al., "Accurate measurement of the optical constants n and k for a series of 57 inorganic and organic liquids for optical modeling and detection," *Appl. Spectrosc.* **72**(4), 535–550 (2018).

9. A. K. Goyal et al., "Active infrared multispectral imaging of chemicals on surfaces," *Proc. SPIE* **8018**, 80180N (2011).

10. M. T. Eismann, *Hyperspectral Remote Sensing*, p. 458, SPIE Press, Bellingham, Washington DC (2012).

11. J. Theiler et al., "Spectral variability of remotely sensed target materials: causes, models, and strategies for mitigation and robust exploitation," *IEEE Geosci. Remote Sens. Mag.* **7**(2), 8–30 (2019).

12. B. E. Bernacki et al., "Modeling liquid organic thin films on substrates," *Proc. SPIE* **10629**, 1062916 (2018).

13. C. J. Breshike et al., "Infrared backscatter imaging spectroscopy of trace analytes at stand-off," *J. Appl. Phys.* **125**, 104901 (2019).

14. B. M. DeVetter et al., "Optical and chemical characterization of uranium dioxide ($UO_2$) and uraninite mineral: calculation of the fundamental optical constants," *J. Phys. Chem. A* **122**, 7062–7070 (2018).

15. T. L. Myers et al., "Quantitative reflectance spectra of solid powders as a function of particle size," *Appl. Opt.* **54**(15), 4863–4875 (2015).

16. J. E. Moersch and P. R. Christensen, "Thermal emission from particulate surfaces: a comparison of scattering models with measured spectra," *J. Geophys. Res.* **100**(E4), 7465–7477 (1995).

17. G. Raz et al., "Novel trace chemical detection algorithms: a comparative study," *Proc. SPIE* **10198**, 101980D (2017).

18. M. Born and E. Wolf, *Principles of Optics*, 6th ed., pp. 40–41, Pergamon Press, Oxford (1986).

19. T. L. Myers et al., "Accurate optical constants for liquids in the near-infrared: improved methods for obtaining the n and k constants from 1 to 4 $\mu$m," *Proc. SPIE* **11010**, 110100O (2019).

20. T. L. Myers et al., "IARPA/PNNL liquid phase IR spectra," NIST Chemistry Webbook, 2018, https://webbook.nist.gov/chemistry/silmarils-liquids-n-k/ (accessed 12 April 2019).

21. J. E. Bertie, "Quantitative infrared intensities of neat liquids: their measurement and use," *Microchim. Acta Suppl.* **47**, 15–22 (1997).

22. J. E. Bertie et al., "Infrared intensities of liquids XI: infrared refractive indices from 8000 to 2 $cm^{-1}$, absolute integrated intensities, and dipole moment derivatives of methanol at 25°C," *Appl. Spectrosc.* **47**, 1100–1114 (1993).

23. B. M. DeVetter et al., "Single-angle reflectance spectroscopy to determine the optical constants n and k: considerations in the far-infrared domain," *Appl. Opt.* **57**(22), 6587–6597 (2018).

24. M. R. K. Kelly-Gorham et al., "Complex refractive index measurements for $BaF_2$ and $CaF_2$ via single-angle infrared reflectance spectroscopy," *Opt. Mater.* **72**, 743–748 (2017).

25. T. A. Blake et al., "Measurement of the infrared optical constants for spectral modeling: n and k values for $(NH_4)_2SO_4$ via single-angle reflectance and ellipsometric methods," *Proc. SPIE* **10198**, 101980J (2017).

26. H. Fujiwara, *Spectroscopic Ellipsometry: Principles and Applications*, John Wiley and Sons, San Francisco, California (2007).

27. T. L. Myers et al., "Obtaining the complex optical constants *n* and *k* via quantitative absorption measurements in KBr pellets," *Proc. SPIE* **11010**, 110100M (2019).

28. T. A. Blake et al., "Methods for quantitative infrared directional-hemispherical and diffuse reflectance measurements using an FTIR and a commercial integrating sphere," *Appl. Opt.* **57**(3), 432–446 (2018).

29. K. Dewitt, "Advances in active infrared spectroscopy for trace chemical detection," *Proc. SPIE* **10986**, 109860J (2019).

30. T. L. Myers et al., "Accurate measurement of the optical constants for organic and organophosphorous liquid layers and drops," *Proc. SPIE* **10629**, 1062912 (2018).

31. Lambda Research Corporation, "TracePro," Version 20.2, http://www.lambdares.com/tracepro (2020).

32. A. Macleod, *Thin-Film Optical Filters*, 3rd ed., Institute of Physics, Bristol (2001).

33. D. Rakić, "Algorithm for the determination of intrinsic optical constants of metal films: application to aluminum," *Appl. Opt.* **34**, 4755–4767 (1995).
34. M. Rubin, "Optical properties of soda lime glasses," *Sol. Energy Mater.* **12**(4), 275–288 (1985).
35. "Physical constants of organic compounds," in *CRC Handbook of Chemistry and Physics*, D. R. Lide, Ed., CRC Press, Boca Raton, Florida, Internet Version, 2005, http://www.hbcpnetbase.com (2005).
36. R. N. Clark and T. L. Roush, "Reflectance spectroscopy: quantitative analysis techniques for remote sensing applications," *J. Geophys. Res.* **89**(B7), 6329–6340 (1984).

**Bruce E. Bernacki** received his PhD in optical sciences from the University of Arizona. Prior to joining Pacific Northwest National Laboratory, he spent nearly 5 years as a vice president of New Product Development and CTO at LightPath Technologies, in Orlando, FL. His experience includes optical design, modeling, optical data storage, and optical component manufacturing. He has received two R&D 100 awards in 2014 and 2017 for his inventions.

**Timothy J. Johnson** is a *cum laude* graduate of Carleton College and received his PhD in chemical physics from Washington State University in 1987. He is currently a senior scientist at PNNL and has extensive experience with spectroscopic signatures, including contributions to the PNNL gas-phase database and other high fidelity spectroscopic signature efforts including for solids and liquids. He has led efforts for better quantitation using visible and infrared reflectance, as well as Raman spectroscopy. He is a member of the SPIE, Optical Society of America, and a recent corecipient of the Meggars Award.

**Tanya L. Myers** is a senior research scientist at PNNL. She received her BS degree in chemistry from the University of North Carolina at Chapel Hill in 1992 and her PhD in chemistry from the University of Chicago in 1997. From 1997 to 1999, she was a National Research Council Postdoctoral fellow at the National Institute of Standards and Technology in Boulder, CO. Her current research interests include high-resolution infrared spectroscopy and quantitative measurement of the optical constants for stand-off detection of solids and liquids. She is a member of SPIE, Optical Society of America, and Phi Beta Kappa.